Flow, Turbulence and Combustion (2021) 106:81–108
https://doi.org/10.1007/s10494-020-00157-7

Combined Blowing/Suction Flow Control on Low-Speed Airfoils

Vladimir Kornilov[1]

Received: 2 December 2019 / Accepted: 28 April 2020 / Published online: 1 August 2020

Abstract
The paper focuses on the application of the blowing/suction technique to control incompressible turbulent boundary layer on 2-D low-speed airfoils. Analysis of the experimental and numerical results obtained with the combined flow control technique through the high-technological perforated sections is carried out. This control method turns out to be a more effective way to improve aerodynamic performance of airfoil compared to isolated forcing. Such technology allows us in the studied conditions to provide an effect, characterized by an increase in the airfoil lift and, ultimately, an increment in lift-to-drag ratio $\Delta K/K_{\max}$ by about 0.06. For all combinations of the control forcing, the simplified mechanism responsible for changes in the airfoil aerodynamic performances is almost identical: the pressure increases due to blowing on one side of the airfoil and decreases due to suction on the opposite side, thus, leading to enhancement of the lift force and, as a consequence, to a gain in the lift-to-drag ratio. Also evaluation of the efficiency of the considered control technique with allowance for energy expenses is given.

Keywords Turbulent flow control · Blowing/suction · Airfoil · Aerodynamic performances

1 Introduction

Further progress of high-speed air transport and on-ground transportation is hardly possible without the development of new cost-efficient methods of controlling near-wall turbulent flows (Abbas et al. 2013; Wood 2004; Ashill et al. 2005). Currently available experience of Laminar Flow Control (LFC) (Lord et al. 1995; Barry et al. 1994) is a good starting point for the development of effective methods acting on the turbulent boundary layer. However even laminar flow, despite its apparent simplicity (especially those at high Reynolds numbers), is rather difficult for investigations. Thin Laminar Boundary Layers (LBLs) are extremely sensitive to minor defects of the tested surface (Bushnell 2003). Such defects can appear as a result of inevitable industrial tolerances in the aircraft structure, the presence of junctions of various aerodynamic elements such as wing/body, and also

✉ Vladimir Kornilov
kornilov@itam.nsc.ru

[1] Laboratory of Experimental Aerogasdynamics, Khristianovich Institute of Theoretical and Applied Mechanics SB RAS, Novosibirsk, Russia

contamination by insects and defects induced by collisions of the leading edge of the wing, nose part of the fuselage, and engine nacelles with small particles of sand or garbage. It is not accidental that various approaches have been investigated by numerous researchers to protect the leading edge against insect contamination. Obviously, these problems can become aggravated in the case of control actions in the form of suction as the boundary layer thickness decreases. Therefore, the LFC as applied to the airplane as a whole and to the wing in particular is a challenging problem.

At the same time it is well known that the boundary layer on many flying vehicle-elements, such as the aircraft fuselage, the rocket airframe, and even the wing, is in the turbulent state within a wide range of Reynolds numbers. As illustrated in Fig. 1 (Hills 2005), almost 50% of overall drag based on a typical A320 aircraft is due to the viscous drag, which consists of pressure-drag portion, as well due to viscous effects, like the displacement of the free stream by the growing boundary-layer thickness. It is evident that fraction of the lift-induced drag reaches approximately 1/3 in the total balance of viscous drag. This fact stimulates research aimed at studying the possibility of improving the aerodynamic performances of the wing. Therefore, the use of artificial methods of turbulent flow control on the wing is considered as one of encouraging ways, which can reduce friction drag and total drag, thus, increasing the lift-to-drag ratio of the flying vehicle. As a consequence, the flight range and payload can be increased, whereas the expenses for the fuel and direct operating costs can be reduced.

The scope of the current paper, related to the steady-state flow control, does not allow us to consider the whole variety of these control methods, in particular synthetic jets, although they include the processes of blowing and suction (Abbas et al. 2013; Wood 2004). It is clear that a general overview of different control techniques would require another detailed article. The technology of near-wall flow control by means of blowing and suction dates back to the early 1950s and was used in some experiments already at that time (Dannenberg and Weiberg 1952; Weiberg and Dannenberg 1954), and others. This technology has been further developed in a number of the works (Simpson et al. 1969; Simpson 1970; Kays and Moffat 1975), performed on flat surfaces using permeable materials obtained by the powder-metallurgy technology. Not so long ago, new developments in micro technology

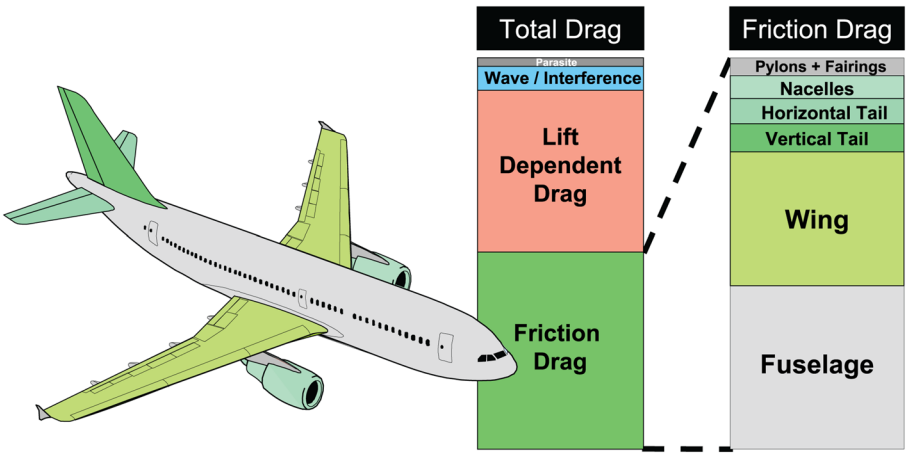

Fig. 1 Typical breakdown of the overall aircraft drag by form and component (based on a typical A320). Adopted from Hills (2005)

and improved manufacturing processes are enabling new concepts for active flow control to be realized, hence creating new opportunities for the control of turbulent boundary layer. Among these methods, turbulent flow control by means of micro-blowing of the gas through a high-technology finely perforated permeable flat surface (Hwang 2004; Tillman and Hwang 1999; Lin et al. 1998; Li et al. 2009; Kornilov and Boiko 2012, 2014; Kornilov 2015) looks fairly attractive.

Technologies of isolated forcing (blowing or suction) for boundary layer control on the flat plate are well known in practice of laboratory investigations (Hwang 2004; Lin et al. 1998; Kornilov 2015; Ferro et al. 2017; Kametani and Fukagata 2011; Kametani et al. 2015). In the general case, the main goal of using these technologies is to remove low-energy fluid layers (by means of boundary layer suction through slots or holes in the surface) or to speed-up these low-energy fluid layers (by means of blowing a high-energy fluid into the boundary layer). In the last case, the high-energy fluid injected to the boundary layer displaces the low-velocity fluid from the wall, thus, leading to friction drag reduction. The energy expenses here can turn out to be somewhat lower, but they have still to be taken into account anyway. By means of blowing, it is even possible to reach negative values of skin friction. This was clearly demonstrated by numerical simulations (Fahland et al. 2019) performed for various airfoil types. However, the penalty for this effect is significant growth of the drag component induced by pressure forces, which is greater than the corresponding value in the baseline flow.

As applied to the flow around the airfoil, the strategy remains essentially the same. The objective of the flow control on airfoils is an attempt to manipulate a particular flow field with a small energy input typically aiming to increase the lift and reduce the drag, to enhance the mixture of momentum, energy, and to suppress the flow-induced noise. In this case, however, the control process is complicated by the formation of a nonequilibrium (according to Clauser) turbulent flow, possible flow separation, and other effects. (According to Clauser, it should be remind, that a boundary layer is in equilibrium state when there is a balance between the processes of generation and dissipation of the kinetic energy of turbulence. However, turbulent boundary layer is often in a nonequilibrium state, for example, at small distances from the beginning of its development, and especially when a sign-variable pressure gradient appears along the chord.) The presence of the above factors often leads to ambiguous influence of blowing or suction on the aerodynamic performances of the airfoil. For example, a change in the blowing region position with respect to the airfoil chord or the angle of attack may significantly alter the properties of the modified flow; as a result, optimal blowing in one situation may turn out to be counter-productive in another scenario. For this reason, it is difficult to develop a unified methodology, which could be successfully used for blowing/suction control on different airfoil types.

It is worth noting that the methods of the flow control in most investigations were mainly used to study the possibility of preventing flow separation at high angles of attack in order to improve the wing's aerodynamic efficiency. Moreover, the majority of investigations was aimed at studying the efficiency of blowing or suction through a transversely oriented single slot. In particular, the influence of air blowing and suction strength on the aerodynamic performances of the airfoil was studied using both numerical (Huang et al. 2004; Yousefi et al. 2014) and experimental (Al-Battal et al. 2018; Kornilov et al. 2019a) methods for different Reynolds numbers, ranges of angles of attack, slot positions, and other parameters. The results of these works are outside the topic of the present article.

The issues of using permeable surfaces for flow control on an airfoil, which have important applications in practice, have not been adequately studied. There are very few investigations focused on the efficiency of this flow control technique under conditions

with no separation, more exactly, in the range of cruising angles of attack. As an example, we can mention the study by Eto et al. (2019), where the effects of uniform blowing on a Clark-Y airfoil are investigated experimentally with the aim of turbulent friction drag reduction. The authors used two types of permeable materials: a porous metal plate with the porosity of 15% and mean pore diameter $d = 15$ μm, and a perforated metal plate with the hole diameter $d = 0.5$ mm. The uniform blowing was applied at the rear part of the upper surface. The experiment was carried out at the free-stream velocity $U_\infty = 58$ m/s, and the Reynolds number based on the chord length was $\mathrm{Re}_c = 1.5 \times 10^6$. The angle of attack was set to $\alpha = 0°$ and 6°. This study confirmed about 20–40% local friction drag reduction due to blowing. Unfortunately, however, the total drag estimated from the wake pressure profile was found to increase slightly due to blowing.

Concerning the technology of the combined action on the boundary layer, i.e., blowing and suction simultaneously, there are only few laboratory investigations. Moreover, it is assumed that this method of flow control is less effective at the small angles of attack. However, the experience of Kornilov et al. (2018) under above mentioned conditions shows that there are still reserves that have not been used. Therewith, in according to the author no sufficiently accurate measurements were available in the literature concerning distributed steady blowing/suction on airfoils. The distributed method of boundary layer control is understood here as uniform (over the area) blowing or suction performed through a surface area of unlimited length, in particular, through a perforated, porous, or some other surface.

A detailed numerical analysis of the flow state and the lift and drag components on the NACA 4412 airfoil was recently performed by Atzori et al. (2019) in the case of uniform blowing on the pressure side and uniform suction on the opposite side for $\mathrm{Re}_c = 0.2 \times 10^6$. The well-tested code, fine computational mesh (with a total of 216 million nodes), and careful formulation of the boundary conditions allowed the authors to obtain the following result within the framework of the LES model. It has been found an increase in the aerodynamic efficiency C_L/C_D of 2.3% for suction intensity 0.1% U_∞ and 4.6% for intensity 0.2% U_∞. However efficiency C_L/C_D is reduced by 6.3% and 11% when applying blowing with the above intensity.

In view of the foregoing, the main goal of the present study is to achieve in an experiment higher efficiency with a comparatively low intensity of the control action, i.e. by using distributed blowing through the high-technological perforated section and additional suction through similar finely perforated section on the opposite side of the airfoil. It seems important to study both the combined effect of these control techniques on the aerodynamic properties of the airfoil, and interaction of air blowing/suction with the turbulent boundary layer under conditions of an non-uniform adverse pressure gradient.

In conclusion, it should be noted that transition control has significantly different effects compared to the present study as with respect to blowing rates so subsequent drag savings. For this reason, as an alternative solution to the present study, the combined method of boundary layer control may be more effective for naturally developing flows on the airfoil. Numerical simulations of such a flow on the 2D-RAE2822 supercritical airfoil at $\mathrm{M}_\infty = 0.734$ (Cai and Gao 2015) show that the aerodynamic performances of the airfoil at $\alpha = 0°$ can be significantly improved by changing the position of the microporous section along the airfoil and delaying the boundary layer transition. For suction with the coefficient $C_s = 0.008$ at the upper surface, and blowing with the coefficient $C_b = 0.05$ at the lower surface of the increasing the lift coefficient up to 26% and decreasing the drag coefficient down to 15% may be reached.

2 Test Conditions and Computation Procedure

2.1 Wind-Tunnel Model and Setup

The experiments were carried out in subsonic low-turbulence wind tunnel T-324 at the Khristianovich Institute of Theoretical and Applied Mechanics SB RAS (ITAM SB RAS), having $1\times1\times4$-m test-section dimensions, at free stream velocity $U_\infty=21$ m/s, which corresponds to the chord-based Reynolds number $\mathrm{Re}_c=0.7\times10^6$ ($\mathrm{Re}_1=1.4\times10^6$ m^{-1}). Sketch of the airfoil model in the wind tunnel is shown in Fig. 2. The model under study was the symmetrical 4 digit NACA 0012 airfoil of relative thickness $t/c=0.12$. The wing was manufactured from moisture-resistant wood, except for tail part, which was made of metal; it had a symmetrical airfoil with chord $c=501$ mm, span $z=930$ mm, and maximum thickness $t=60$ mm. The trailing-edge thickness was about 1 mm. The main structural elements of the wind-tunnel model in the plan view (a), and in the longitudinal section (b), as well as the scheme of air blowing/suction through the perforated section (c) are shown in Fig. 3. The static pressure orifices of 0.4 mm in diameter were located on both sides of airfoil along its central chord.

It is known that many airfoils, including the NACA 0012 may be particularly sensitive to Reynolds number variations if no trip is used. Therefore to initiate the turbulent boundary layer, two self-adhesive tapes with a medium grain size (their substrate did not of itself effect transition) are placed at $x/c=0.05$ on the windward and leeward sides of the wing. (Here, x-axis is aligned with the airfoil chord.) When choosing the tripping device on airfoil, a number of considerations should be taken into account. First of all, the boundary layer in the measurement flow region should be in equilibrium (according to Clauser) state. Partly for this reason, Gregory's experience (Gregory and O'Reilly 1973) was mainly taken into account when choosing the size and position of the tripping device. According to Gregory, on the lower surface of the NACA 0012 airfoil, where the pressure distributions

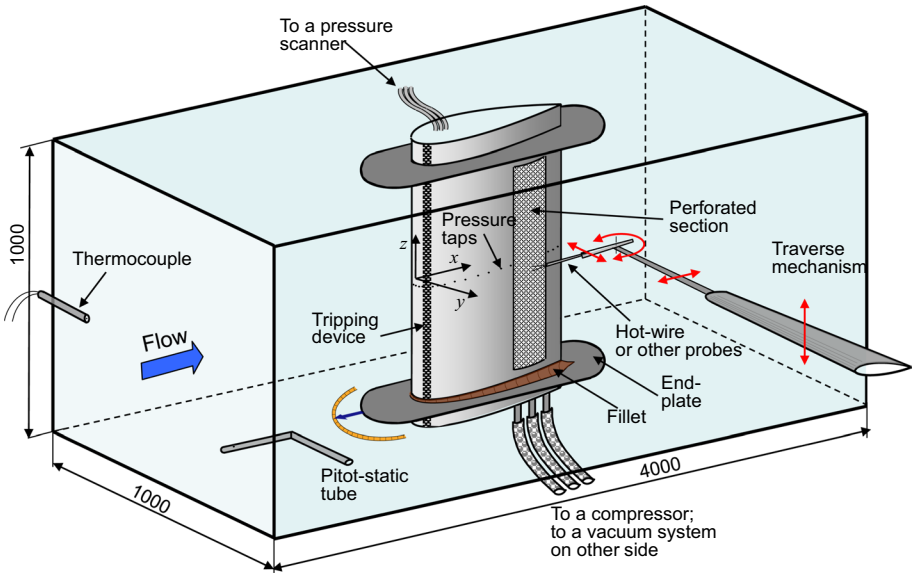

Fig. 2 Sketch of the airfoil model in the wind tunnel

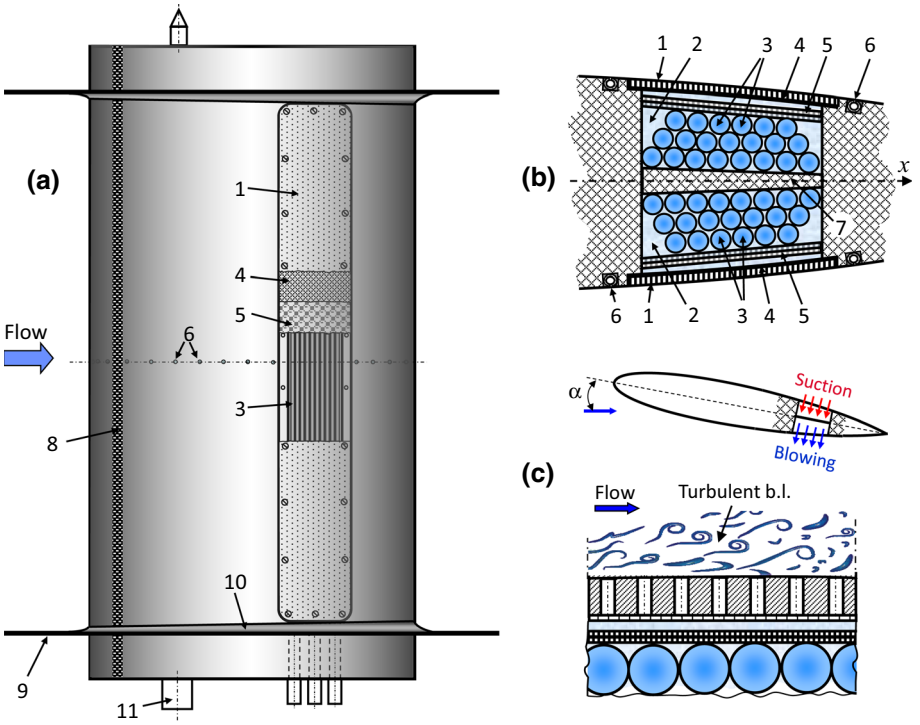

Fig. 3 Basic structural elements of the wind-tunnel airfoil model: **a** plan view, **b** view in the longitudinal section, and **c** scheme of air blowing/suction. (1) perforated section, (2) blowing (suction) chamber, (3) inlet channels for air blowing (suction), (4) fine-mesh filter, (5) two-layer controlled permeability mesh, (6) pressure taps, (7) baffle, (8) boundary-layer tripping device, (9) end-plates, (10) fillet, (11) axis rotation of the airfoil by the angle of attack. Drawing not to scale

were favourable at positive angles of attack, transition at $\mathrm{Re}_c = 1.44 \times 10^6$ moved back from 0.1 chord to mid-chord when the angle of attack increased from 8° to 12°. In this case, 0.3 mm strips, extending for 25 mm over the surface and located 0.1 chord downstream of the airfoil leading edge were used as transition devices. In our case, in order to move the stagnation point as close as possible to the airfoil-leading edge at the larger angles of attack, as well as taking into account the difference in the Re_c, the tripping height (together with the substrate) was increased to 0.6 mm while maintaining other parameters. This was followed by a number of tests before a satisfactory tripping geometry was finally obtained on the airfoil.

It is also well known that when testing in a wind tunnel, it is very difficult to assure two-dimensional conditions of flow around an airfoil. In our case 2D-flow is ensured as far as possible using the end-plates. Remaining induced drag is neglected. However, in the regions of joint of the end-plates with the wing surface, presenting typical corner configurations, there formed a three-dimensional flow with the streamwise developing vortices. To suppress the adverse action of these vortices on the main flow region, the wing fillets were used; the geometry of the fillets was chosen based on Kornilov's data (2017). Measurements of the mean velocity in the cross section $x/c \approx 0.95$ at different spanwise locations showed that two-dimensional flow conditions at $\alpha = 6°$ are provided with a discrepancy of

not more than 5–7%. Thus, we limit our consideration to 2-D airfoils and exclude circulation control and jet-flapped airfoils. Of course, it does not mean that the aerodynamic performances of such airfoil are similar to the same for the wing with larger aspect ratio. The primary cause is that in general case the presence of end-plates leads to a reduction of the section drag coefficient compared to the airfoil without end-plate.

The porosity level of the perforated material, which characterizes the total normalized area of the free cross section of orifices 0.17 mm in diameter, arranged in a staggered order to the total surface area is approximately 18%. The ratio of the orifice diameter to the baseline boundary-layer thickness in front of the permeable insert, for instance at $\alpha = 0°$ is 1/35. The positions of the leading x_l and trailing x_t edges of the perforated regions were chosen to be $0.623c$ and $0.775c$ from the leading edge of the airfoil. The following considerations were used as a basis for choosing the parameters of the perforated section. It is known (Hwang 2004; Kornilov 2015) that the perforated surface should satisfy a certain set of the minimum requirements: high quality of surface finishing, required normalized thickness t/d, elevated uniformity of arrangement of orifices, optimal diameter, and sufficient degree of permeability. It is only if these requirements are satisfied that one can hope that the initial boundary layer (in the absence of blowing or suction) would possess the properties of the classical boundary layer, which could serve as a starting point for studying the characteristics of the modified flow on the airfoil. It is extremely important that the flow past the perforated wall should be equivalent to the flow past a hydraulically smooth analog. In our case both the mean and the rms boundary-layer velocity profiles on the perforated section under the condition without blowing/suction show good agreement with those on the hydraulically smooth surface. On the other hand, the results of the analytical calculation (Abzalilov 2008) indicate how important the optimal position of the permeable wall portion is. Therefore, when choosing the position of the perforated section, the data of both numerical (Huang et al. 2004; Yousefi et al. 2014) and experimental (Al-Battal et al. 2018; Goodarzi et al. 2012) studies were taken into account. In accordance with the results obtained in them, mentioned characteristics can be improved by blowing or suction air through a slot located near the trailing edge of the wing.

Two autonomous sealed chambers, arranged symmetrically on the opposite sides of the airfoil were used for air blowing (suction). To provide uniformity of the air blowing or suction over the insert surface, the chambers design were repeatedly upgraded and improved. Each chamber included cylindrical input channels (21 thin-walled tubes) uniformly distributed over the length and width of the chambers. The uniformity of air blowing (suction) over the wing span z was additionally ensured by using a two-layer controlled permeability mesh, and a fine-mesh filter mounted directly beneath the permeable insert.

2.2 Measuring Methodology and Instrumentation

All probes (Prandtl tube, static pressure tube, hot-wire probe) could be mounted in a traverse mechanism attached to the WT side wall. Therefore, for the convenience of measurements in the boundary layer and in wake, the airfoil was located vertically in the plane of symmetry of the WT test section. By the way, we note that the boundary-layer thickness on the WT side walls in the region of airfoil position is about 28 mm.

Mainly, in order to avoid a significant influence of the WT side walls on the measurement results, most experiments were limited to a range of the angles of attack α from $-6°$ to $+6°$. However, the properties of the boundary layer in front of the perforated section were not studied for all values α. These studies at the selective angles of attack

shown, that the tripping was always below or near the stagnation point. In addition, no significant relaminarization of the flow during suction in the above range of angles of attack was revealed.

Key measurements were performed with the help of a completely automated remotely controlled traverse mechanism with two degrees of freedom (x, y). The instantaneous velocity at the examined point of the shear flow was measured using a set of the DANTEC 55M0 single-component constant-temperature hot-wire anemometer. The setup of the anemometer included the 55M10 hot-wire bridge, for which the output signal was conditioned by the 55D10 linearizer. The signal from the linearizer was fed to the L-CARD E-440 multichannel high-frequency 14-digit external A/D converter, which transferred the digitized data through a universal serial bus port to a computer. The data at each measurement position were acquired during 15 s with a sampling frequency of 10 kHz. The constant component of the linearized signal, corresponding to the mean flow velocity, was measured in parallel using a 55D31 digital dc voltmeter. A low-pass filter was used throughout the experiment to filter out high-frequency noise from the hot-wire output signal. The filter was set at 20 kHz for all measurements. A miniature hot-wire probe with a single sensor made of tungsten wire with a diameter of 5 μm and an active length of 1.2 mm was used as a primary measurement transducer, which operated in the constant temperature mode with an overheating of 1.7. The probe was produced by special technology developed at the ITAM SB RAS. In measuring, the probe touched the wall by the tips of the prongs of about 56–60 μm in diameter. Thus, the distance from the wall to the middle of the wire diameter was constant and equal to 28–30 μm. To avoid possible mistakes due to inaccurate determination of the initial position of the wire relative to the wall, the touch of the hot-wire prongs to the airfoil surface was controlled during the experimental runs using a special optical cathetometer with improved spatial resolution. The estimated measurement accuracy of this procedure was ± 3 μm. The cooling effect of the wall on the hot-wire anemometer readings was also taken into account (Boiko and Kornilov 2010).

In determining the coefficient of airfoil profile drag C_D, being the sum of the friction drag and pressure drag, for some reasons, we preferred using the well-known momentum method (Jones 1936):

$$C_D = \frac{2}{c}\int_{y_1}^{y_2}\sqrt{\frac{P_{0w}-P_w}{P_0-P_\infty}}\left(1-\sqrt{\frac{P_{0w}-P_\infty}{P_0-P_\infty}}\right)\mathrm{d}y \tag{1}$$

i.e.,

$$C_D = \frac{2}{c}\int_{y_1}^{y_2}\phi(y)\mathrm{d}y. \tag{2}$$

Here, $\varphi(y)$ is the integrand, with $(P_{0w}-P_w)$ being the difference between the total and static pressure in the wake and (P_0-P_∞) the difference between the total and static pressure in the free stream. The pressure differences were measured, respectively, with a miniature Prandtl tube 2 mm in diameter located at a distance of 152 mm ($0.303c$) from the trailing edge of the wing, and with a standard Prandtl tube routinely used for performing measurements in the wind tunnel. The lift coefficient was determined from the results of integration of the distribution of pressure on the airfoil surface measured by pressure sensors:

$$C_L = \int_0^1 (C_{p_w} - C_{p_l}) \mathrm{d}\bar{x} \tag{3}$$

where the subscripts "w" and "l" at the coefficient C_p refer, respectively, to the windward and leeward sides of the wing. A typical appearance of the function $\varphi(y)$ for different angles of attack can find, for instance in Kornilov (2018).

The random error in the experimentally determined values was evaluated from five successively performed measurements. The pressure profiles measured across the airfoil wake with subsequent determination of the integrand showed, in particular, that the error in the determination of the drag coefficient σC_D did not exceed $\pm 3.5\%$. Note, however, that this error does not take into account possible systematic errors, which, for various reasons, may arise during the experiment and which are most often uncontrolled.

It should be noted that the blowing (suction) coefficient $C_{b,s}$ is often used in the literature as a typical parameter that characterizes the strength of the injected or sucked jet. In the 2D case, it has the form

$$C_{b,s} = \rho_{b,s} V_{b,s} / \rho_\infty U_\infty, \tag{4}$$

where the subscripts "b" and "s" refer to blowing and suction. In the 2D incompressible flow Eq. (4) reduces to

$$C_{b,s} = V_{b,s} / U_\infty. \tag{5}$$

In the following we will use this parameter to interpret the results of researches. In our case $V_{b,s}$ is average (over the area) blowing or suction velocity to be determined from the flow rate measurements. The total airflow rate was measured with an electronic mass flow meter of AALBORG (model GFM 67) in the range 0–500 of standard liters per minute with an error less than 1.5% of the maximum value.

2.3 Boundary Conditions, Mesh Design, and Simulation Procedure: validation

The final computations were performed within the framework of the ANSYS Fluent software system by means of solving two-dimensional steady Reynolds-averaged Navier–Stokes equations (2D RANS) with the two-parameter k–ω SST turbulence model. Justification for choosing this turbulence model is provided below. A steady state simulation was performed under the assumption of a fully developed turbulent boundary layer starting from the leading edge of the airfoil. The availability of the boundary-layer tripping device on the airfoil was not taken into account. Discretization of both the conservation and transport equations was performed using the upwind scheme. The gradients in the conservation equations were computed using the second-order approximation of derivatives by the Green-Gauss Cell-Based method. The turbulence transport equations were computed using first-order derivatives approximation by the Green-Gauss Cell-Based method. Thus, the method of discretization for both the conservation and transport equations is the same, and the computational mesh is also the same. However, the accuracy of computing the flow parameters (pressure, velocity) and turbulence parameters (k, omega) differs due to the different accuracy of the approximating the derivatives in the corresponding equations. The convergence of the solution was estimated on the basis of residual differences, which, depending on particular parameter, were equal to 10^{-8}–10^{-4} when the problem solution

was finalized, as well as on the basis of the balance of the mass flow rate through the computational domain boundaries (2×10^{-8}–4×10^{-8} of the mass flow rate through the inlet boundary).

The computational domain is a rectangle with the airfoil model at the center (Fig. 4). The domain geometry is chosen in such a way as to ensure 2D simulation of a subsequent WT experiment with boundary layer control by means of blowing and suction. The distances from the inflow boundary of the computational domain to the leading edge of the wing and from the trailing edge of the wing to the outflow boundary are 9 and 8 chord lengths, respectively. The distances to the left and right (side) boundaries of the computational domain are equal to one chord length (they are bounded by the WT side walls). It is clear that the influence of the WT side walls would be much less when the shape of these walls had been adapted to the shape of a streamsurface according to non-viscous theory of the infinite wing flow. In our case, the flat side walls of the WT test section are simulated in RANS. The structured computational mesh consists of 5.2 million quadrangular cells. The model is refined toward the model surfaces so that the known dimensionless parameter y^+ in the near-wall layer should stay in the interval 0.1–0.2. The same mesh is maintained at the inlet to the WT test section up to a distance of about one chord from the leading edge of the airfoil and at the outlet from the WT. When the angle of attack changes, the mesh near the airfoil surface rotates together with the airfoil. The only difference is that in the region area between the airfoil neighborhood and the WT wall boundaries, different meshes have differences of about 20–30% of the volume of the WT test section. The inflow boundary was subjected to the mean free-stream velocity and turbulence parameters. The turbulence intensity was 0.05% of the mean velocity value, and the ratio of the turbulent and molecular viscosity coefficients was chosen to be equal to unity. The inlet boundary condition in RANS regarding the turbulent intensity corresponds to that measured in the wind tunnel. This seems quite acceptable here, since no transition is investigated and turbulent kinetic energy-production delay in boundary layer is only weakly depends on free stream

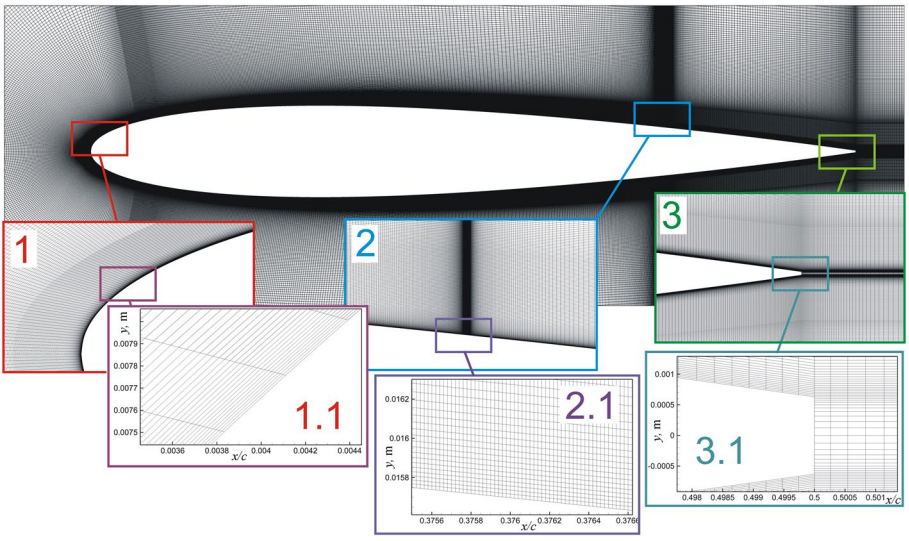

Fig. 4 Details of mesh topology at the flow around NACA 0012 airfoil (example with slot located at the distance $x/c=0.75$)

turbulence. The airfoil trailing-edge thickness in RANS simulation similar to that on the wind tunnel model. The no-slip condition was imposed on the upper and lower boundaries of the computational domain corresponding to the WT walls. The outflow boundary of the computational domain was subjected to "soft" boundary conditions calculated as the mean-weighted values between the flow parameters inside the computational domain and the reference parameters at the outflow boundary. This means that when computing, the boundary conditions are changed at each iteration step, gradually adapting to the flow inside the computational domain, so that in the end of the solution they become matched with the solution inside of computational domain (for example, the outflow velocity is become nonzero). This was possible based on the following approach. For example, to calculate the flow parameters in a layer of cells adjacent to the right boundary of the computational domain, we used the boundary condition called by the developers of the ANSYS Fluent software system "Pressure Output". In accordance with this, the reference values of static pressure, turbulence intensity, and the ratio of turbulent and molecular viscosity were assigned to the right boundary of the computational domain. The values of the flow velocity from the adjacent inner region were extrapolated to the boundary itself. The pressure in the layer of cells adjacent to the boundary was calculated as the mean-weighted value between the pressure inside the computational domain and the reference value by the fifth-order of accuracy. The turbulence parameters at the boundary were calculated similarly. Thus, the considered boundary condition is close to the classical definition of the Dirichlet boundary condition. The reference pressure at the outflow boundary was set equal to standard atmospheric pressure of 101,325 Pa. The turbulence reference parameters were chosen to be identical to those at the inflow boundary.

It should be only noted here that the computational algorithm was simplified. It was not possible to solve the problem in the exact formulation, since the turbulence characteristics of the experimental air supply system into the holes of the perforated surface are unknown. Partly, for this reason, the perforated section of the surface was replaced by a periodic set of slots 0.09 mm wide with a step of 0.41 mm along the chord. The slot size and the number of slots were chosen in such a way that the total perimeter of the slots should be approximately equal to the total perimeter of all holes in the wind-tunnel experiment. Our experience related to some other tasks shows that the initial level of turbulence (boundary conditions for k and ω) in the flow core at the nozzle exit (in our case, at the exit of the slot) affects the parameters of the jet-mixing layer from the nozzle (slot) significantly less than the choice of the turbulence model itself.

For obtaining a correct solution of the considered problem, the computational algorithm has to be tested. In similar cases, much attention is usually paid to choosing reliable experimental data free from any noticeable errors and also representative criteria for comparisons of turbulence models. It was done by comparing the drag coefficient C_D for the NACA 0012 airfoil with reliable experimental data of Abbott and Doenhoff (1959), and Ladson (1957), obtained for the flow around this airfoil with a zero lift force and generalized by McCroskey (1987) using Eq. (6)

$$C_D = 0.0017 + 0.91/\left(\lg \mathrm{Re}_c\right)^{2.58}. \tag{6}$$

These data are highly valuable because they were obtained under conditions of the developed turbulent boundary layer in the absence of any noticeable influence of the WT walls; moreover, the experimental values C_D were measured in the case with artificial tripping of the boundary layer on the model. Judging by the dependence $C_D = f(\lg \mathrm{Re}_c)$ (Fig. 5), the current numerical data for the free-stream conditions (red circles) agree well with the

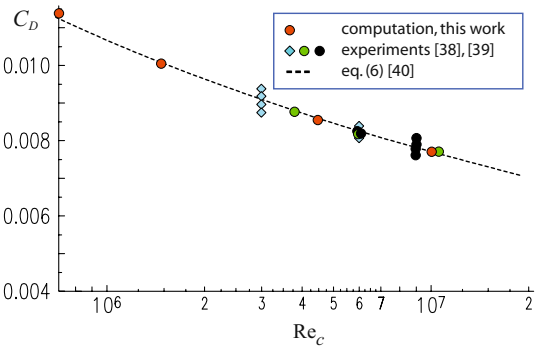

Fig. 5 Comparison between the computational and experimental (Eq. 6) drag coefficients for NACA 0012 airfoil

results predicted by the generalized formula given above. It follows from here that a structured mesh that takes into account flow specifics to a needed extent is fairly sufficient for obtaining an acceptable solution for an unbounded flow around the NACA 0012 airfoil.

However different turbulence models, as well as their different combinations with various numerical schemes, could lead to qualitatively different predictions for airfoil flows. Meanwhile, very few information reflecting the process of searching for a correct turbulence model for calculating turbulent flows on airfoils is available in publications. Normally, the final results obtained with the turbulence model that ensured the best agreement with the experiment are reported.

The drag coefficients C_D for the NACA 0012 airfoil in the free flow with different Reynolds numbers computed with the use of the k–ω SST, k–ω, k–ε Realizable EWT, and Spalart–Allmaras turbulence models are given in Table 1. A comparison of the values of C_D predicted with the use of the k–ω SST model reveals their reasonable agreement with the experimental data of McCroskey (1987) (Eq. 6). Vice versa, the k–ε model yields more significant differences from the experimental data. This fact is quite understandable because this model is more suitable for the free turbulence description, whereas the k–ω model ensures acceptably accurate results in near-wall regions. Thus, the most accurate model was the k–ω SST model, second came the Spalart–Allmaras model, and in the worst precision was provided by the Realizable k–ε model. By the way, the advantages of the k–ω SST model were noted in some publications (Douvi et al. 2012) dealing with computations of the flow on airfoils in a wide range of variation of the angle of attack α at subsonic velocities. The current study also justifies the use of the SST model with pressure-gradient turbulent boundary layers (Vinuesa et al. 2014).

The results of similar testing, performed by comparing the computational results with experimental pressure distribution on the wing surface (see Gregory and O'Reilly 1973) under conditions close to those in unbounded (free) flow, also showed satisfactory

Table 1 Comparison between experimental data based on Eq. (6) and four different turbulence models simulation results of the drag coefficient for NACA 0012 airfoil

$\mathrm{Re}_c \times 10^{-6}$	0.725	1.45	2.9	10
By Eq. (6)	0.01120	0.01005	0.009083	0.007707
k–ω SST	0.01127	0.01020	0.00911	0.007843
k–ε real. EWT	0.01414	0.01216	0.01055	0.008467
k–ω	0.01361	0.01094	0.009326	0.007370
Spalart–Allmaras	0.01281	0.01157	0.01054	0.008985

convergence. Thus, if necessary requirements to the mesh design, in particular, to the number of nodes and mesh density, boundary conditions, and computational algorithm on the one hand and to the relative dimensions of the airfoil on the other hand are satisfied, numerical simulations yield a fairly adequate pattern of the flow around the baseline airfoil NACA 0012.

3 Results

3.1 Boundary-Layer Characteristics

The presence of a pressure gradient (especially sign-changing) along the streamlined surface can significantly affect the formation of the flow structure on the airfoil. In this regard, it seems important to consider the behavior of the boundary layer along the chord of the baseline wing in the presence of the WT bounding walls.

The chordwise change of the most important characteristics of the boundary layer is shown in Fig. 6 for $\alpha = 0°$ in the form Re** (x/c) and $H(x/c)$, where Re** is the Reynolds number calculated from the momentum thickness, and $H = \delta^*/\delta^{**}$ is the shape factor. As can be seen, there is an intensive increase in the value of Re**, intensifying with increasing coordinate x. At the same time, the growth rate of the shape factor H is weak, and the values themselves, other conditions being identical, are close to the corresponding magnitudes on a flat plate. Also it is particularly important that the boundary layer on the baseline airfoil is in the developed turbulent state, which is evidenced by the profiles of the integral intensity of velocity fluctuations u'_{rms} in the boundary layer (Fig. 7) whose maximum magnitude is approximately 8.6% of the mean flow velocity; other conditions being identical, this magnitude is close to the corresponding magnitude for a flat plate (Kornilov and Boiko 2012). Thus, the nature of the flow on the baseline wing seems to be quite natural. Moreover, judging by the measured velocity profiles, the boundary layer on the studied profile develops without any features and has a non-separated character in the range of angles of attack $\alpha = -6° \div 6°$. Indeed, Fig. 8, which shows the experimental profiles of the mean velocity $U/U_{pw} = f(y)$ in the boundary layer on the sides of blowing and suction in the cross section $x/c = 0.7$ corresponding to the middle of the perforated section, confirms this fact. Here U_p is the mean flow velocity, which is not fixed, but depends on the normal coordinate (see, the fragment in Fig. 8b.) It is determined on the basis of the parameter

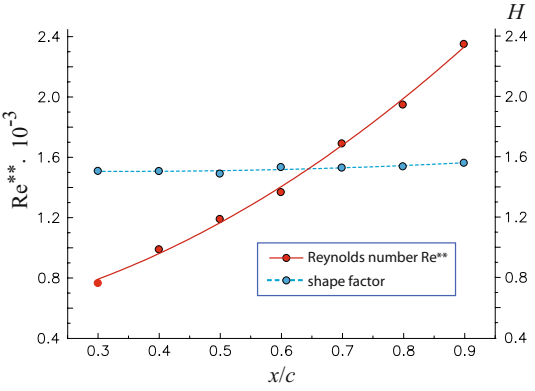

Fig. 6 Chordwise momentum-thickness Reynolds number Re** and shape factor distributions

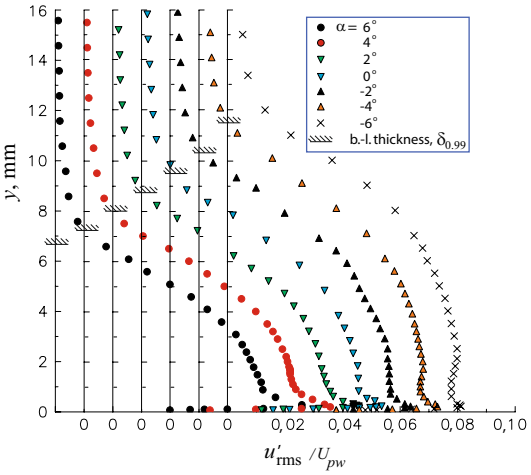

Fig. 7 Streamwise rms velocity fluctuation profiles in the cross section $x/c = 0.7$

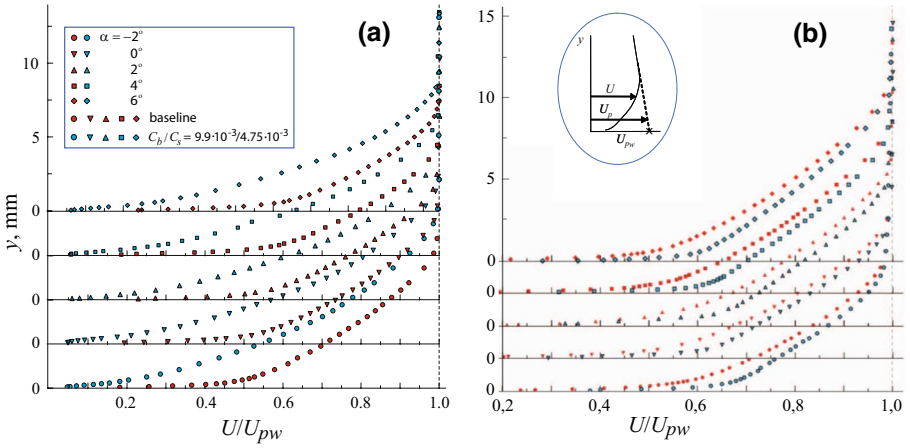

Fig. 8 Streamwise mean velocity profiles on the blowing side (**a**) and on the suction side (**b**) in the cross section $x/c = 0.7$

U_{pw}, which is called the "velocity of the potential flow on the wall" (So and Mellor 1973; Meroney and Bradshaw 1975). In turn, the value of this parameter was found by means of extrapolation of the linear part of the profile outside the boundary layer onto the surface. The choice of this scaling is due to the following reason. As a rule, the flow velocity at the edge of boundary layer U_e is used to scale the velocity in a conventional gradientless turbulent boundary layer. However, at the flow around airfoil, the local flow velocity in an experiment differs from the corresponding magnitude in the free stream flow even at a large distance from the wall. In this case, the local flow velocity outside the boundary layer asymptotically approaches the velocity in the free stream, but due to influence of the WT walls, often don't reaches it. It follows that the mean velocity in the boundary layer is more convenient to scale in terms of the U_{pw} quantity.

As expected, in the case of blowing (Fig. 8a), the velocity profiles for all angles of attack are less filled as compared to those for the baseline configuration. Vice versa, in the case of

suction (Fig. 8b), the mean velocity distribution over the boundary layer height displays the opposite character. Naturally, the velocity gradient near the wall, which reflects the behavior of the friction component, decreases in the first case and increases in the second one. The above-noted properties of the modified flow are confirmed by the mean velocity distribution inside the boundary layer plotted in the law-of-the-wall coordinates $U^+ = f(y^+)$

$$U/v_*, y^+ = yv_*/\nu, \tag{7}$$

where ν is the kinematic viscosity and $v_* = (\tau_w/\rho)^{1/2}$ is the friction velocity. It is clear that the dimensionless velocity U^+ increases in the case of blowing and, vice versa, decreases in the case of suction. Note, by the way, that the mean velocity profile in the law-of-the wall variables over the perforated section at zero mass flow rate is described quite satisfactorily by the law of the wall for a hydraulically smooth surface, as shown by the authors (Kornilov et al. 2019b). This gives reason to believe that in this chordwise position the turbulent boundary layer is in equilibrium (according to Clauser) state. The numerical analysis (Atzori et al. 2019) of the flow around the NACA 4412 airfoil in the cross section $x/c = 0.8$ for uniform blowing and suction also reveals a continuous increase in U^+ in the case of blowing and its decrease in the case of suction as the control action intensity is enhanced. This tendency is caused by the decrease in the shear stress τ_w and, hence, in the friction velocity v_* in the first case and their increase in the second case.

In the case of suction (Fig. 9), the values of u'_{rms} permanently decrease over the entire boundary layer height y. The reason is obvious: the gas masses, which have a reduced level of turbulence in the outer region of the boundary layer, are transferred toward the wall. Moreover, even this comparatively moderate flow rate of sucked air can initiate the transport process covering the entire height of the boundary layer. This fact is qualitatively consistent with the experimental results (Ferro et al. 2017) for a flat plate, which testifies to a certain analogy in the two types of the flows in the case of suction.

In the case of blowing (Fig. 10), similar to the flat plate case (Kornilov and Boiko 2012, 2014), the character of the distribution of turbulent fluctuations of velocity over the boundary layer height y is rather ambiguous. In this case, enhancement of velocity fluctuations is observed in the major part of the boundary layer, except for a narrow near-wall region $0 \le y \le 0.5$ mm ($0 \le y/\delta_{0.99} \le 0.07$), where $\delta_{0.99}$ is the boundary layer thickness determined from the condition $U/U_{pw} = 0.99$. A decrease in u'_{rms} (Fig. 11) caused by displacement of

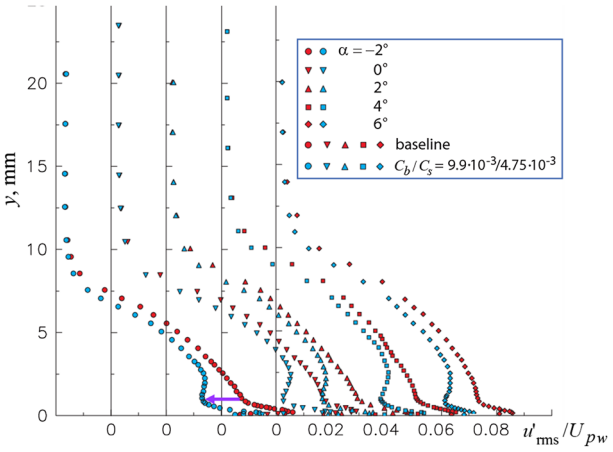

Fig. 9 Streamwise rms velocity fluctuation profiles on the suction side in the cross section $x/c = 0.7$

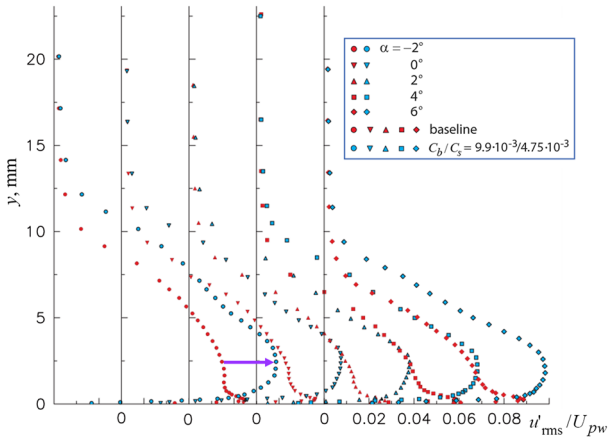

Fig. 10 Streamwise rms velocity fluctuation profiles on the blowing side in the cross section $x/c = 0.7$

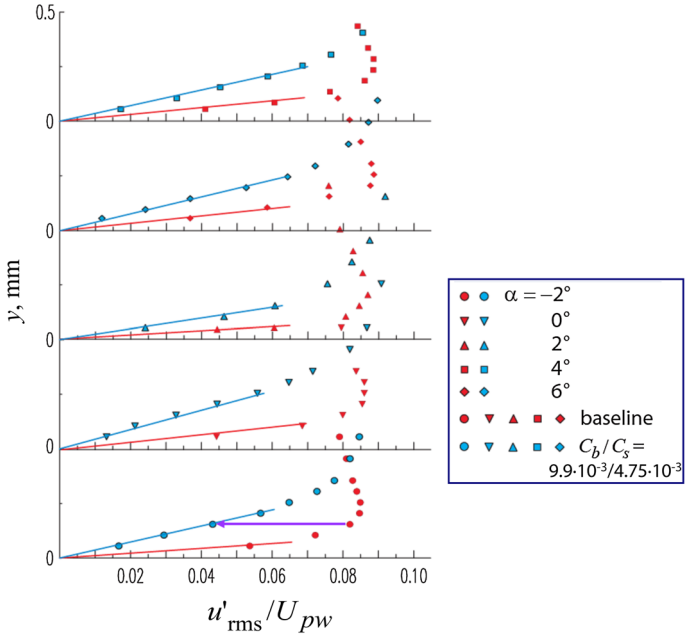

Fig. 11 Streamwise rms velocity fluctuation profiles, limited by the small magnitudes of the wall-normal coordinate y on the blowing side in the cross section $x/c = 0.7$

the gas mass with elevated turbulence from the wall is observed in this region. According to Eto et al. (2019) the rms velocity fluctuations in the region close to the airfoil surface are increased due to the blowing. However, they are also shifted up from the surface, which indicates that turbulence near the surface is suppressed by blowing. The results of the numerical analysis (Atzori et al. 2019) for uniform blowing and suction reveal an identical dynamic pattern of the behavior of the streamwise component of velocity fluctuations across the boundary layer.

The computed contours of the velocity magnitude and streamlines in the vicinity of the airfoil at a zero angle of attack and under a combined control action in the form of blowing/suction (Fig. 12) as a whole do not have any particular specific features. However, it is worth noting that a disturbed flow region is formed above the perforated section from the side of blowing (lower surface) (Fig. 12b). In a recent study (Mahfoze et al. 2018) a similar effect was detected for the normal component of velocity and local friction in the flow past a flat plate by means of direct numerical simulation. A possible reason is a strong adverse pressure gradient arising upstream of the blowing region. This is true because the main flow is blocked near the wall and is deflected upwards, thereby increasing the normal component of velocity above the blowing region. It follows from here that a further increase in the flow rate of air blowing is hardlfy reasonable, at least from the viewpoint of airfoil drag reduction. View versa, from the side of suction (upper surface), there are no signs of the formation of such disturbed regions, though it should be borne in mind that the values of C_s here are smaller than the values of C_b.

At the same time, despite the good residuals due to the extremely fine computational mesh, there are some artifacts in the wake (Fig. 12a) which are possibly not steady. The role and influence of these artifacts on the properties of the flow in the boundary layer and the aerodynamic performances of the wing are discussed in the analysis of Fig. 14.

3.2 Aerodynamic Performances

Information of the influence of certain parameters on the aerodynamic performances of airfoils under the conditions of blowing or suction uniformly distributed over the surface is extremely scarce. Therefore, the discussion below is based on results of a few studies, which were not very consistent or systematic. The experience of such investigations as applied to the NACA 0012 airfoil allows brief formulation of the results in the following way.

First of all, it should be noted that the aerodynamic characteristics $C_D(\alpha)$ and $C_L(\alpha)$ of the baseline airfoil NACA 0012 (Fig. 13) do not contain essential specific features at first

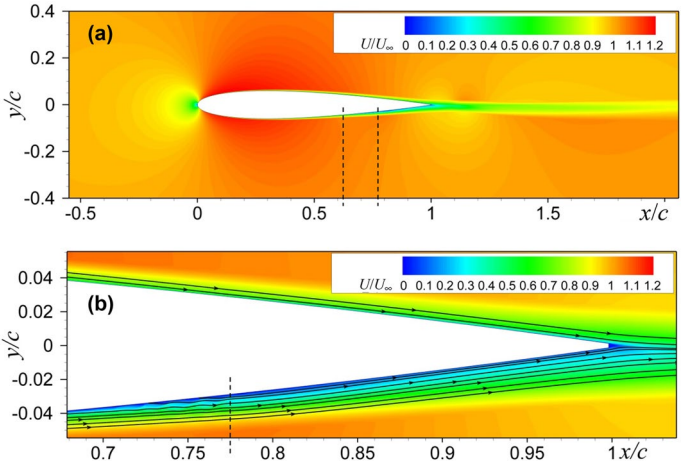

Fig. 12 Computed velocity contours and streamlines for the flow around NACA 0012 airfoil for the blowing/suction coefficients $C_b/C_s = 9.9{\cdot}10^{-3}/4.75{\cdot}10^{-3}$: **a** Whole model and **b** model tail part. Dashed lines are the boundary of perforated surface

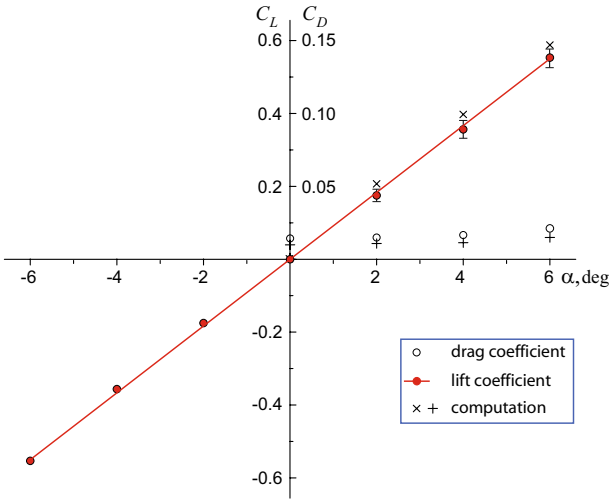

Fig. 13 Experimental and computational drag and lift coefficients versus the angle of attack for NACA 0012 airfoil

glance. In particular, the behavior of the dependence $C_L(\alpha)$ is close to linear, thus, providing certain similarity to the classical theory of thin wings. However, the deviation of experimental data from numerical predictions tested for free-stream conditions is outside the error range. (Here, the random error of experimental values was estimated based on the results of their five-fold successively performed measurements.) A particularly significant difference reaching 30% is observed for the drag coefficient C_D. This difference may be attributed to the error of airfoil mounting in the WT, error of measurement tools, and presence of boundary layer tripping devices, which definitely cause problems in experimental modeling of the flow around airfoils. However, the main problem, as shown by numerical simulations, is caused by interference of the airfoil model with the WT walls. There are a number of the results which support this statement. Among them, a study by Bui and Lapygin (2015), which evaluated the above factors for the T-324 wind tunnel. Within a numerical study, these authors found that with a certain ratio between the geometric parameters of the NACA 0012 airfoil and the size of the test area, the difference in the drag coefficients obtained under WT conditions and free (unbounded) flow conditions, i.e., with no influence of the tunnel wall, can reach 50% at the angle of attack $\alpha = 12°$. When the angle of attack decreases, this difference decreases, but it still remains large. Moreover, the difference in the lift coefficients C_L can reach 20%. According to the authors, the main reason for this is interference between the airfoil and WT walls.

Figure 14 shows the computed pressure fields (Fig. 14a–d) and mean velocity fields (Fig. 14e–h) in the vicinity of the NACA 0012 airfoil at $\mathrm{Re}_c = 0.7 \times 10^6$ for some selected angles of attack α. The computational domain geometry, mesh parameters, and conditions on the computational domain boundaries were chosen in accordance with the above-described technology. Unsurprisingly, when the angle α increases, the pressure on the windward side increases, and the pressure on the leeward side decreases. At $\alpha = 12°$, direct measurements revealed the presence of a weakly expressed pressure plateau, which testifies to the beginning of separated flow formation near the trailing edge on the leeward side of the airfoil. However it can be noted that at a distance from the WT walls to the wing of the order of one chord ($y/c \approx \pm 1$), an interference effect takes place, which is noticeable even at small angles of attack α (Fig. 14a, b), and markedly amplifying at $\alpha = 8°$ and 12° (Fig. 14c,

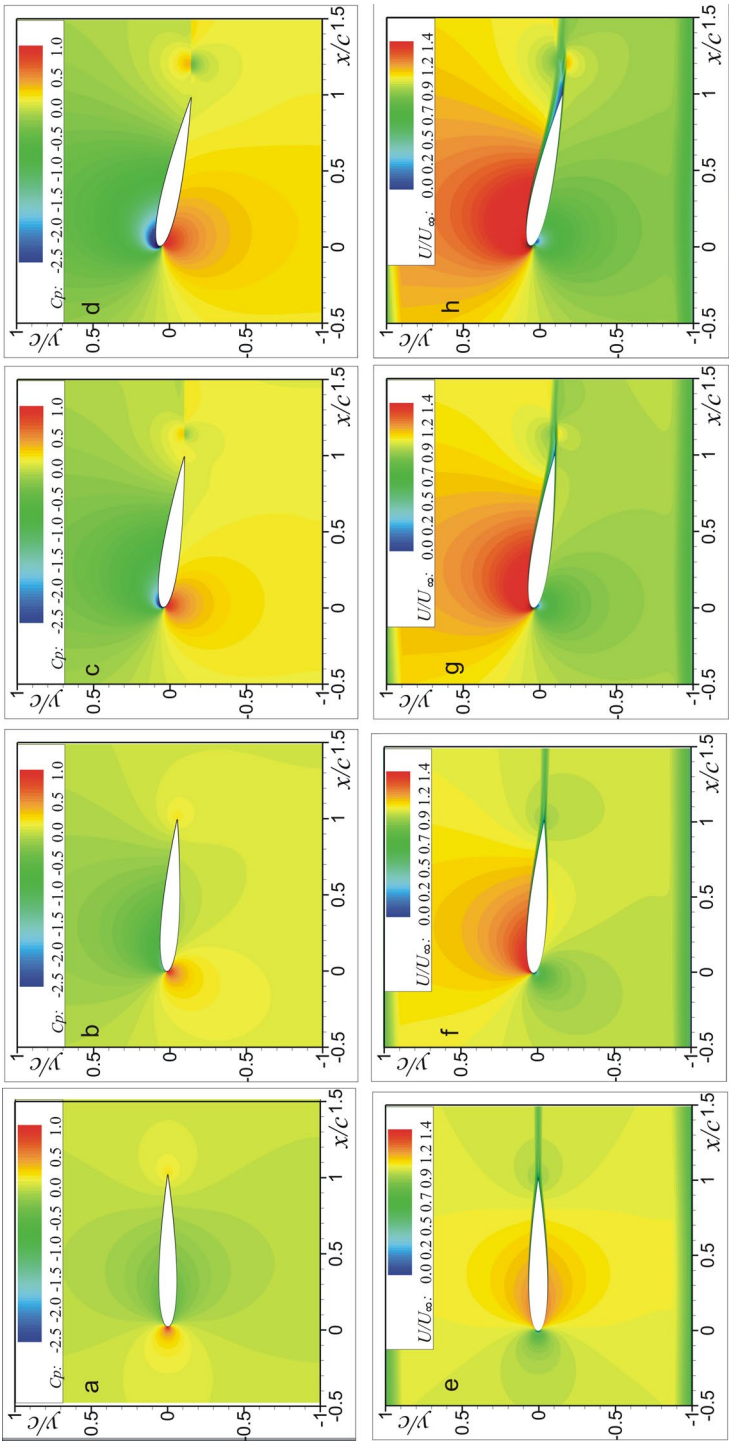

Fig. 14 Contours of the mean pressure coefficient **(a–d)**, and mean streamwise velocity **(e–h)** for the flow around NACA 0012 airfoil for $Re_c = 0.7 \times 10^6$. Angle of attack α, deg: 0 **(a, e)**, 4 **(b, f)**, 8 **(c, g)**, 12 **(d, h)**

d). This leads to a corresponding increase in the pressure level on the leeward side of the airfoil in the experiment, and, as a result, to a greater extent of the non-separated local region formed in the vicinity of the model-trailing edge.

There are methods that, in principle, allow the WT measurement results to be corrected, e.g., by introducing corrections to flow blockage by the model and cocurrent jet. At the same time, according to the author the recommended in literature correction coefficients are not quite reliable. Therefore, they are seldom used in practice; most researchers try to use flow regimes where these effects are definitely low. Taking this fact into account the mentioned correction was not made in our case. Thus, systematic error in aerodynamic coefficients C_D and C_L can be explained mainly by the blockage effect of airfoil in the WT test section.

Again, we pay attention to the existence in the wake behind the airfoil of some artifacts that may indicate unsteadiness. To clarify this phenomenon, additional analysis at the different angles of attack was carried out. For this, special investigations have been done to obtain information if these artifacts move when calculating some more iterations. (By the way, in all cases the solution turned out to be convergent within the residual differences.) As a result, the effect of these artifacts on the flow around the airfoil was revealed. In this case, the regular pressure pulsations of relatively small amplitude arise in the vicinity of the airfoil. However, in the range of angles of attack from $-6°$ to $6°$, the rms deviation of the aerodynamic coefficients $S_d(C_L)$ and $S_d(C_D)$, due to these pulsations, from the average values C_L and C_D does not exceed thousandths of a percent. With a further increase in α, the rms deviations $S_d(C_L)$ and especially $S_d(C_D)$ become more significant. For angles $\alpha = 8°$ and $12°$ the $S_d(C_D)$ values turned out to be 17% and 20%, respectively. The deviation in the lift coefficient $S_d(C_L)$ even with an angle of attack of $12°$ does not exceed 2.0%. The influence of these pulsations on the integral properties of the flow and the averaged aerodynamic performances of the wing can be considered insignificant.

In the case of isolated air suction from the boundary layer through a finely perforated wall (without blowing), the greatest reduction of the drag coefficient C_D of the NACA 0012 airfoil at $\mathrm{Re}_c = 0.7 \times 10^6$ is reached for the maximum value of the suction coefficient C_S equal to 4.75×10^{-3} (Fig. 15). The measurements show that suction leads to constriction of the wake part of the flow behind the airfoil, which is an indirect sign of reduction of the drag component induced by pressure forces. It is worth noting, however, that the interval of preferable values of C_S is bounded approximately by the value of 1.5×10^{-3}. A further increase in the suction coefficient for the perforated section position chosen in the study

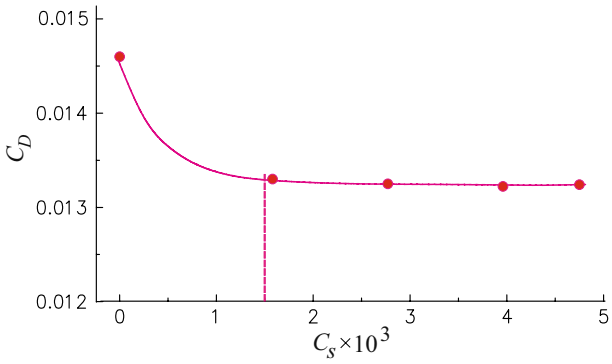

Fig. 15 Drag coefficient versus the suction coefficient C_s for $C_b = 0$

seems to be not reasonable because it can only lead to an increase in energy expenses. It is of interest that Atzori et al. (2019) discovered an almost identical character of the dependence $C_D(C_S)$, which reveals the most prominent reduction of C_D in the initial range of the values of C_S and an extremely weak growth or even its stabilization with a further increase in C_S.

At the same time additional studies recently performed by the author clearly show that there is a reserve for improving the aerodynamic performances of the airfoil. A number of the design changes, including modification of the airfoil model have been undertaken, first of all, to improve the air blowing (suction) system by reducing its hydraulic drag. Let us remark by the way, that efficiency of the blowing/suction technology on board, for instance on an aircraft to a considerable extent depends on the mentioned system, the optimization of which is of great importance. Indeed, Fig. 16, which shows the change in aerodynamic drag of the airfoil in the form of the dependence $\Delta C_D/C_{D0/0}=f(\alpha)$, where $\Delta C_D=(C_D-C_{D0/0})/C_{D0/0}$ ($C_{D0/0}$ refers to the baseline airfoil), confirms this fact. As can be seen more than 15% drag reduction can be obtained by suction. It is important to emphasize that this effect is achieved at an angle of attack $\alpha=-6°$, i.e. with the suction on the leeward side of the airfoil. This implies that suction is more efficient on the airfoil side, where the prerequisites to the formation of a separated flow arise. It should also be noted that an increased suction coefficient leads to a decrease in pressure ahead of the perforated section, but the increase in the lift coefficient is rather weak again. It is clear that uniform suction yields to a lower velocity in the wake and weaker wall-normal convection.

Concerning the isolated blowing effect, a minor decrease in the drag coefficient C_D of the airfoil occurred only in the initial range of C_b. A continuous growth of C_D was observed with a further increase in the blowing coefficient. Therefore, blowing as an independent method of boundary layer control is not of much interest, at least for the perforated section position along the airfoil declared here. The growth of the drag component induced by pressure forces prevails in the total balance of forces over the reduction of the drag component induced by skin friction. It is not accidental that Atzori et al. (2019) did not observe any gain in C_D for blowing coefficient $C_b>0.001$.

Of particular interest is the combined effect (blowing/suction) on the aerodynamic performances of the airfoil. The results show that the drag coefficient C_D can be reduced approximately by 10% by using small values of the blowing coefficient C_b and constant

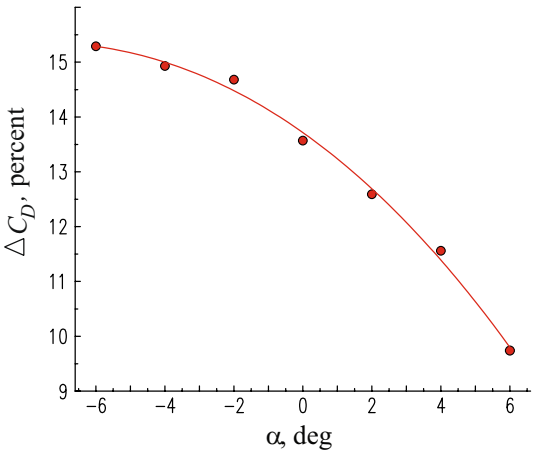

Fig. 16 Drag coefficient versus the angle of attack α for suction coefficient $C_s=7.85\times10^{-3}$ ($C_b=0$)

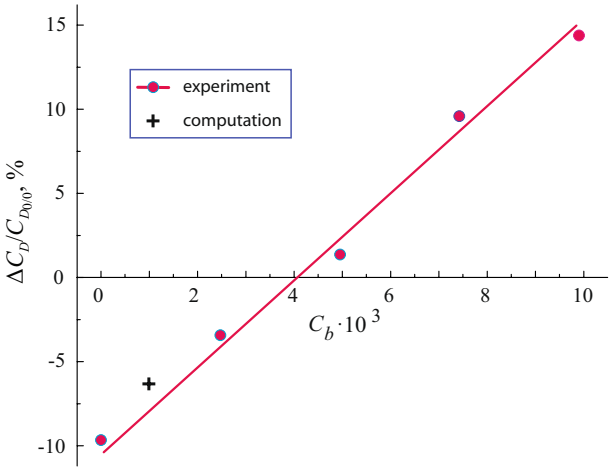

Fig. 17 Drag coefficient versus the blowing coefficient for the suction coefficient $C_s = 4.75 \times 10^{-3}$

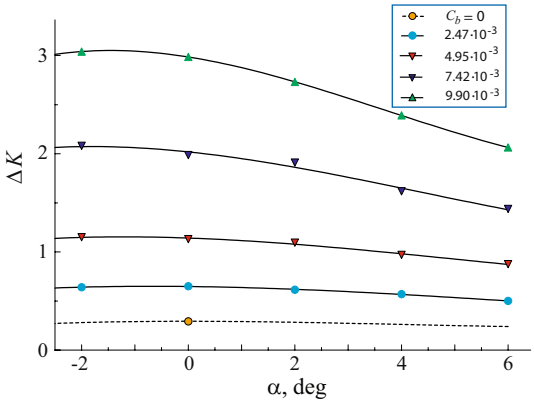

Fig. 18 Lift-to-drag ratio versus the angle of attack α for the suction coefficient $C_s = 4.75 \times 10^{-3}$

suction (Fig. 17). As the C_b increases, the drag coefficient begins to increase and exceeds the corresponding value for the baseline airfoil when a certain value of C_b is reached. The change in the drag coefficient, presented here in the form $\Delta C_D/C_{D0/0} = f(C_b)$, where $\Delta C_D = (C_D - C_{D0/0})/C_{D0/0}$, clearly shows that this method of boundary layer control, at least for given conditions, becomes ineffective at $C_b > 4 \times 10^{-3}$.

Thus, for the chosen position of the perforated section, whose leading and trailing edges are located at distances $0.623c$ and $0.775c$, respectively, the main result can be formulated as follows. In the total force balance, suction exerts a minor effect on the lift force, but assists in airfoil drag reduction, whereas blowing ensures an almost linear growth of the lift force. As a result, the combined method of flow control can provide an increase the in lift-to-drag ratio ΔK of the NACA 0012 airfoil at a level of three units. Since $K_{\max} \approx 50$ for this airfoil at $\mathrm{Re}_c = 0.7 \times 10^6$ (Gregory and O'Reilly 1973), then $\Delta K/K_{\max} \approx 0.06$. The curve $\Delta K = f(\alpha)$, plotted in Fig. 18 for the variable blowing coefficient and constant suction shows the maximum increment of the lift-to-drag ratio at different angles of attack α. At a higher angle of attack, the efficiency of this method of boundary layer control is lower. The main reason can be formulated as follows: with an increase

in α, the natural growth of pressure C_p on the windward side of the airfoil becomes a dominating factor as compared to the additional growth of C_p caused by blowing. For comparison, it can be noted that according to Atzori et al. (2019) the increase of the skin friction is countervailed by a higher decrease of the pressure drag and improvement of lift, which lead to an increase of the aerodynamic efficiency of 2.3% for suction intensity 0.1% U_∞ and 4.6% for intensity 0.2% U_∞.

In general, based on studies with different blowing and suction values, an interesting conclusion can be drawn. Various combinations of blowing and suction that ensure identical flow rates of air can lead to different final effects.

As for optimal flow control, this is a complex multi-parameter task, especially with regard to the combined method. The difficulty lies in the fact that it is necessary to obtain the optimal values of a number of parameters for various airfoil geometries and blowing/suction conditions. It is clear that the experiment is too expensive to solve such a problem. In this regard, the need arose, for a long time, to create a comprehensive database of aerodynamic sensitivity of the parameters involved in the design process. In this context, computational fluid dynamics is an extremely attractive tool. Verification of the numerical solution by comparing with experimental results at control points with subsequent analysis in the entire region of the studied parameters seems to be the most optimal way.

3.3 Simplified Flow Control Mechanism

The above-noted increment in the lift-to-drag ratio ΔK is reached not only due to drag reduction caused by suction from the boundary layer, but primarily due to lift enhancement mainly caused by blowing. This fact becomes clear if we consider the dependence $C_p = f(x/c)$, which characterizes the pressure distribution over the airfoil surface subjected to the combined forcing (blowing/suction) on the boundary layer (Fig. 19). A comparison with the results for the baseline NACA 0012 airfoil (averaged data) shows that air blowing at the lower side of the airfoil (at constant suction) leads to a pressure increase on this surface, including the region immediately upstream of the blowing point. This is obvious because the normal velocity component induced by blowing blocks the main flow near the wall, thus, acting as an air-jet spoiler. Moreover, the elevated pressure region above the perforated surface itself extends approximately to one half of its length. Then the value of C_p decreases and remains unchanged further downstream from the perforated section.

Vice versa, air suction at the opposite side of the airfoil leads to a pressure decrease on the surface, including the region immediately upstream of the suction range. Naturally, this tendency becomes enhanced with an increase in both C_b and C_S, which is qualitatively consistent with the results of Cai and Gao (2015) for $M_\infty = 0.734$, indicating that C_p displays a somewhat conservative behavior for different flow regimes around the airfoil.

Thus, the physical mechanism that determines the flow character on the airfoil under the action of blowing and suction, regardless of the type of the permeable surface, can be described as follows. The total effect induced by the increase in pressure due to blowing at one side of the airfoil and the decrease in pressure due to suction at the opposite side leads to an increase in the lift force and, finally, in the lift-to-drag ratio. Blowing, as an isolated forcing, actually does not provide drag reduction in the case with the declared position of the perforated section; the main reason of the increase in K is enhancement of the lift force. Moreover, the increment of the lift coefficient is an almost linear function of the flow rate through the perforated wall.

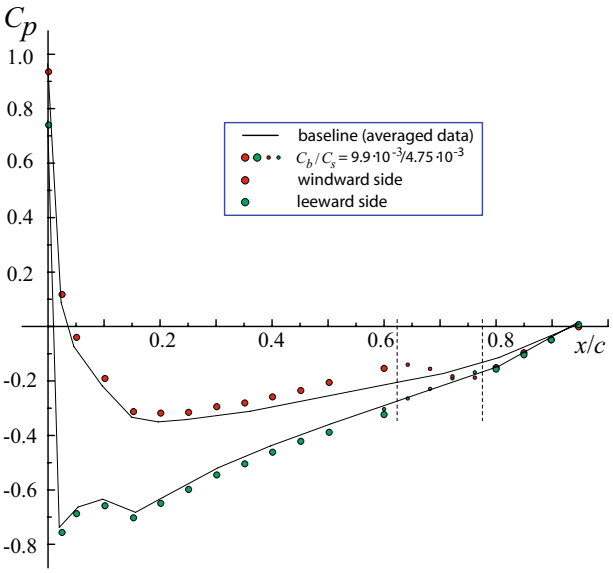

Fig. 19 Typical chordwise pressure coefficient distribution at = 2°. The large and small points show the results measured by the pressure taps and static pressure probes, respectively; the vertical dashed lines indicate the boundaries of the blowing and suction regions

3.4 Estimation of Energy Cost for Air Blowing/Suction

The efficiency of the proposed control method can be estimated in different ways. For example, according to numerical simulations (Ponza et al. 2013), this can simply be done by comparing the increase in the aircraft power due to the use of the onboard control system with the propulsive power gain due to blowing or suction. In estimating the efficiency of the forced method of boundary layer control, in particular, combined control, we assume that the uniform translational motion of the airfoil is ensured by an engine. Under WT test conditions, this is the engine generating a flow with a prescribed velocity. Then the propulsive power, i.e., the projection of the thrust force onto the x axis is

$$N_{\text{prop}} = D_{b,s}U_\infty = 0.5C_{Db,s}\rho_\infty U_\infty^2 U_\infty S, \tag{8}$$

where the subscripts "b" and "s" refer to blowing and suction, respectively, and S is the planform area of the airfoil.

On the other hand, the power spent on blowing and suction can be presented as

$$N_{\text{sup}} = X_{\text{bas}}V_{b,s} = 0.5C_{D\text{bas}}\rho_\infty U_\infty^2 V_{b,s}S, \tag{9}$$

where the subscript "bas" refers to the baseline airfoil.

The total power determined by the propulsive power and the power spent on blowing and suction is

$$N_\Sigma = N_{\text{prop}} + N_{\text{sup}}. \tag{10}$$

On the other hand, the propulsive power of the baseline airfoil can be expressed as

$$N_{\text{bas}} = X_{\text{bas}} U_\infty = 0.5 C_{D\text{bas}} \rho_\infty U_\infty^2 U_\infty S. \tag{11}$$

Then the normalized power characterizing the efficiency of the control method used can be presented as

$$\overline{N} = N_\Sigma / N_{\text{bas}} \tag{12}$$

An example of the estimated efficiency of the combined method of flow control with allowance for energy expenses at the angle of attack $\alpha = 0°$ is shown in Fig. 20 in the form $\overline{N} = f(C_b + C_s)$. It is evident from this figure that the maximum effect of the order of 8% is reached at the total blowing/suction coefficient $(C_b + C_s)$ approximately equal to (0.4–0.5) $\times\ 10^{-3}$. As $(C_b + C_s)$ increases, the efficiency of the method decreases, and the method becomes cost-inefficient at $(C_b + C_s) \geq 1.1 \times\ 10^{-3}$ for the above-mentioned position of the permeable section.

The estimate presented here reflects the specific features of energy expenses on forced blowing/suction in on-ground tests, and it should be considered only as an intermediate stage on the way of application of these results in practice. Obviously, organization of the flow control process on the aircraft wing will require an autonomous source of power; otherwise, the power needed for this purpose will have to be withdrawn from the engine shaft. Therefore, the final conclusion on using the blowing/suction technology can be formulated similar to that for any other method of boundary layer control. If the drag reduction, which is equivalent to fuel saving, is greater than the parasitic component due to expenses on supporting the weight of the power source and conducting system, then the goal can be considered as being reached.

4 Conclusions

- Utilization of the blowing/suction through the high-technological surface, featuring low roughness and maximal requirements to orifice quality and geometry, is a simple, available, and reliable method of the turbulent boundary-layer control on low-speed airfoils in the aerodynamic experiment. This technology allows providing an effect characterized by an increase in the airfoil lift and, ultimately, by a gain in lift-to-drag ratio K reaching a level of three and more units, which in terms of $K_{\max}$ corresponds to a value equal to 0.06.

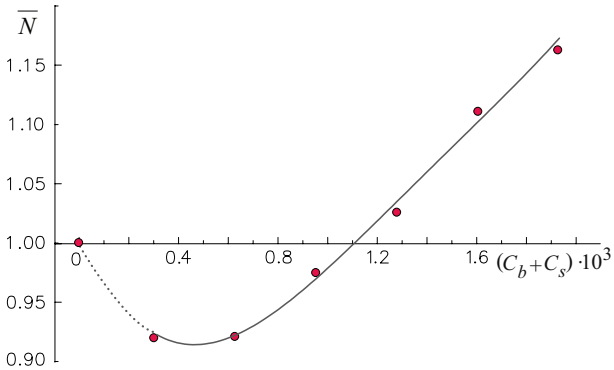

Fig. 20 Relative power versus the overall strength coefficient (blowing/suction) at $\alpha = 0°$

- Results obtained testify to an ambiguous character of the combined effect of steady distributed air blowing/suction on the aerodynamic performances of airfoil. The nature of the effect of blowing and suction on these performances is significantly different. Nevertheless, blowing can be successfully used for changing the lifting properties of airfoil, especially if the air blowing region is located near the trailing edge. Using suction, one can ensure drag reduction, but the effect of suction seems noticeably smaller for the same values of the suction coefficient.
- Mechanism of changing the aerodynamic performances of airfoil under the blowing and suction of various intensities is basically the same. It consists in the fact that an increase in pressure due to the air blowing on one side of the wing and a decrease in pressure due to the air suction on the opposite side leads to an effect characterized by an increase in lift and, ultimately, by a gain in lift-to-drag ratio.
- Combined method of boundary layer control has undoubted advantages, but its potential under developed turbulence conditions has not been yet exhausted, and the efficiency reached cannot be considered as the maximum possible value. A further increase in flow control efficiency can be provided, in particular, by choosing optimal chordwise positions of the blowing and suction regions, as well as their lengths. The latter is of particular importance in practical situations in which, according to the conditions of structural rigidity, only local areas on the wall can be made permeable.
- Blocking effects (among other effects) appear to be one of the important parameters responsible for discrepancies between experimental and numerical results at the flow over airfoils. Although this problem is far from new, but it is especially topical at the application of the blowing/suction control technique on airfoils. This means that blockage effect should be taken into account in recalculation to the free-stream conditions.
- Further progress, when employed given flow control method, can be provided by means of a symbiosis of experiment and numerical computation which takes into account the three-dimensional character of interaction of exhausting (through the perforated wall) microjets with each other and with the boundary layer.
- Final conclusion on the efficiency of flow control by means of blowing/suction can be made only after estimating the inherent energy expenses. To perform professional evaluation of these expenses, it seems reasonable to extend the experimental technique to a level providing a possibility of measuring the total drag of the combination consisting of the airfoil and input air pipelines, which would allow one to obtain a justified estimate of the efficiency of this control method, at least under on-ground conditions.

Funding The work was partially supported by the Russian Foundation for Basic Research (Grant No. 18-08-00256) and by the Program of Basic Scientific Research of the State Academies of Sciences for 2013-2020 (project AAAA-A17-117030610137-0, No. 0323-2018-0005). The author also expresses his sincere gratitude to Dr. Ivan Kavun for helping in computations at each stage of the work performance.

Compliance with Ethical Standards

Conflict of interest The author declares that he has no conflict of interest.

References

Abbas, A., de Vicente, J., Valero, E.: Aerodynamic technologies to improve aircraft performance. Aerosp. Sci. Technol. **28**, 100–132 (2013)

Abbott, I.H., von Doenhoff, A.E.: Theory of Wing Sections Including a Summary of Airfoil Data, pp. 124–187. Dover Publications, New York (1959)
Abzalilov, D.F.: Aerodynamic design and optimization of airfoil shapes in complicated flow schemes. Doctor's dissertation, Kazan (2008) **(in Russian)**
Al-Battal, N., Cleaver, D., Gursul, I.: Lift reduction by counter flowing wall jets. Aerosp. Sci. Technol. **78**, 682–695 (2018)
Ashill, P.R., Fulker, J.L., Hackett, K.C.: A review of recent developments in flow control. Aeronaut. J. **109**(1095), 205–232 (2005)
Atzori, M., Vinuesa, R., Schlatter, P., Gatti, D., Stroh, A., Frohnapfel, B.: Effects of uniform blowing and suction on turbulent wing boundary layers. Proceedings of the European Drag Reduction and Flow Control Meeting (EDRFCM), March 26–29, 2019, Bad Herrenalb, Germany (2019)
Barry, B., Parke, S.J., Brown, N.W., Riedel, H., Sitzmann, M.: The flight testing of natural and hybrid laminar flow nacelles. ASME paper 94-GT-408 (1994)
Boiko, A.V., Kornilov, V.I.: Hot-wire anemometer measurement of local skin-friction coefficient. Thermophys. Aeromech. **17**(4), 613–622 (2010)
Bui, V.T., Lapygin, V.I.: Simulation of the flow past a model in the closed test section of a low speed wind tunnel and in the free stream. Thermophys. Aeromech. **22**(3), 351–358 (2015)
Bushnell, D.M.: Aircraft drag reduction—a review. Proc. Inst. Mech. Eng. Part G. J Aerosp. Eng. **217**(1), 1–18 (2003)
Cai, J., Gao, Z.X.: Numerical study on drag reduction by micro-blowing/suction compounding flow control on supercritical airfoil. Procedia Eng. **99**, 613–617 (2015)
Dannenberg, R.E, Weiberg, J.A.: Section characteristics of a 10.5-percent thick airfoil with area suction as affected by chordwise distribution of permeability. NASA technical note 2847, Ames Aeronautical Laboratory, Moffett Field, CA (1952)
Douvi, C.E., Tsavalos, I.A., Margaris, P.D.: Evaluation of the turbulence models for the simulation of the flow over a National Advisory Committee for Aeronautics (NACA) 0012 airfoil. J. Mech. Eng. Res. **4**(3), 100–111 (2012)
Eto, K., Kondo, Y., Fukagata, K., Tokugawa, N.: Assessment of friction drag reduction on a Clark-Y airfoil by uniform blowing. AIAA J. **57**, 2774–2782 (2019)
Fahland, G., Gatti, D., Frohnapfel, B., Stroh, A., Atzori, M., Vinuesa, R., Schlatter, P.: RANS investigation of blowing and suction for turbulent flow control on a wing section. European Drag Reduction and Flow Control Meeting (EDRFCM 2019), Bad Herrenalb, Deutschland, 26–29, März 2019 (2019)
Ferro, M., Fallenius, B.E., Fransson, J.H.M.: On the turbulent boundary layer with wall suction. In: Progress in Turbulence VII, Springer Proceedings in Physics 196. https://doi.org/10.1007/978-3-319-57934-4_6 (2017)
Goodarzi, M., Rahimi, M., Fereidouni, R.: Investigation of active flow control over NACA 0015 airfoil via blowing. Int. J. Aerosp. Sci. **1**(4), 57–63 (2012)
Gregory, N., O'Reilly, C.L.: Low-speed aerodynamic characteristics of NACA 0012 airfoil section, including the effects of upper-surface roughness simulating hoar frost. ARC Reports and Memoranda 3726, London, UK (1973)
Hills, D.: The Airbus challenge. Aeronaut. J. **109**(1102), 639–644 (2005)
Huang, L., Huang, P.G., LeBeau, R.P.: Numerical study of blowing and suction control mechanism on NACA0012 airfoil. J. Aircr. **41**(5), 1005–1013 (2004)
Hwang, D.: Review of research into the concept of the microblowing technique for turbulent skin friction reduction. Prog. Aerosp. Sci. **40**, 559–575 (2004)
Jones, B.M.: The measurement of profile drag by the Pitot traverse method. ARC R & M 1668 (1936)
Kametani, Y., Fukagata, K.: Direct numerical simulation of spatially developing turbulent boundary layers with uniform blowing or suction. J. Fluid Mech. **681**, 154–172 (2011)
Kametani, Y., Fukagata, K., Örlu, R., Schlatter, Ph: Effect of uniform blowing/suction in a turbulent boundary layer at moderate Reynolds number. Int. J. Heat Fluid Flow **55**, 132–142 (2015)
Kays, W.M, Moffat, R.J.: The behavior of transpired turbulent boundary layers. NASA report HTM-20 (1975)
Kornilov, V.I.: Current state and prospects of researches on the control of turbulent boundary layer by air blowing. Prog. Aerosp. Sci. **76**, 123 (2015)
Kornilov, V.I.: Three-dimensional turbulent near-wall flows in streamwise corners: current state and questions. Progr. Aerosp. Sci. **94**, 46–81 (2017)
Kornilov, V.I.: Control of turbulent boundary layer on a wing section by combined blowing/suction. Thermophys. Aeromech. **25**(2), 155–167 (2018)
Kornilov, V.I., Boiko, A.V.: Efficiency of air microblowing through microperforated wall for flat plate drag reduction. AIAA J. **50**(3), 724–732 (2012)

Kornilov, V.I., Boiko, A.V.: Flat-plate drag reduction with streamwise noncontinuous microblowing. AIAA J. **52**(1), 93–103 (2014)
Kornilov, V.I., Kavun, I.N., Popkov, A.N.: Effect of air blowing and suction through single slots on the aerodynamic performances of an airfoil. J. Appl. Mech. Technol. Phys. **60**(5), 871–881 (2019a)
Kornilov, V.I., Kavun, I.N., Popkov, A.N.: Modification of turbulent airfoil section flow using a combined control action. Thermophys. Aeromech. **26**(2), 165–178 (2019b)
Ladson, C.L.: Two-dimensional airfoil characteristics of four NACA 6A-series airfoils at transonic Mach numbers up to 1.25. NACA reports and memoranda no. L57F05 (1957)
Li, J., Lee, C.-H., Jia, L., Li, X.: Numerical study on the flow control by micro-blowing. 47th AIAA Aerospace Sciences Meeting, Orlando, FL, Jan. 2009. AIAA Paper 2009-779. https://doi.org/10.2514/6.2009-779 (2009)
Lin, Y.L., Chyu, M.K., Shih, T.I.P., Willis, B.P., Hwang, D.P.: Skin friction reduction through micro blowing. AIAA Paper 1998-0359 (1998)
Lord, W.K., Zysman, S.H., Tillman, T.G., Johnson, W.A.: Laminar flow control experiment on a large-scale nacelle model. Pratt &Whitney report PWA 6420-55 (1995)
Mahfoze, O.A., Laizet, S., Wynn, A.: Bayesian optimisation of intermittent wall blowing for drag reduction of a spatially evolving turbulent boundary layer. In: Proceedings of the Tenth International Conference on Computational Fluid Dynamics, Barcelona, Spain, July 9–13, 2018, 1–17 (2018)
McCroskey, W.J.: A critical assessment of wind tunnel results for the NACA0012 airfoil. USAAVSCOM technical report 87-A-5 (1987)
Meroney, R.N., Bradshaw, P.: Turbulent boundary layer growth over a longitudinally curved surface. AIAA J. **13**(11), 1448–1453 (1975)
Ponza, R., Simioni, N., Benini, E.: Numerical assessment of pneumatic devices on the wing/fuselage junction of a tiltrotor. J. Aircr. **50**(3), 752–763 (2013)
Simpson, R.L.: Characteristics of turbulent boundary layers at low Reynolds numbers with and without transpiration. J. Fluid Mech. **42**(4), 769–802 (1970)
Simpson, R.L., Moffat, R.J., Kays, W.M.: The turbulent boundary layer on a porous plate: experimental skin friction with variable injection and suction. Int. J. Heat Mass Transf. **12**(7), 771–789 (1969)
So, R.M.C., Mellor, G.L.: Experiment on convex curvature effects in turbulent boundary layers. J. Fluid Mech. **60**, 43–62 (1973)
Tillman, T.G., Hwang, D.P.: Drag reduction on a large-scale nacelle using a microblowing technique. AIAA Paper 1999-0130 (1999)
Vinuesa, R., Rozier, P.H., Schlatter, Ph, Nagib, H.M.: Experiments and computations of localized pressure gradients with different history effects. AIAA J. **52**(2), 368–384 (2014)
Weiberg, J.A., Dannenberg, R.E.: Section characteristics of an NACA 0006 airfoil with area suction near the leading edge. NASA technical note 3285, Ames Aeronautical Laboratory, Moffett Field, CA (1954)
Wood, R.: Impact of advanced aerodynamic technology on transportation energy consumption. SAE International, technical paper 2004-01-1306 (2004)
Yousefi, K., Saleh, R., Zahedi, P.: Numerical study of blowing and suction slot geometry optimization on NACA 0012 airfoil. J. Mech. Sci. Technol. **28**(4), 1297–1310 (2014)